Hindawi Publishing Corporation
International Journal of Photoenergy
Volume 2012, Article ID 268173, 14 pages
doi:10.1155/2012/268173

Research Article

Effective Sol-Gel Nanocoatings on ZnO Electrodes for Suppressing Recombination in Dye-Sensitized Solar Cells

Shintaro Ueno and Shinobu Fujihara

Department of Applied Chemistry, Faculty of Science and Technology, Keio University, 3-14-1 Hiyoshi, Kohoku-ku, Yokohama 223-8522, Japan

Correspondence should be addressed to Shinobu Fujihara, shinobu@applc.keio.ac.jp

Received 3 February 2012; Accepted 16 April 2012

Academic Editor: David Worrall

Attempts have been made to improve the performance of dye-sensitized solar cells by forming metal-oxide nanocoating layers on ZnO electrodes by a sol-gel transformation. SiO_2, Nb_2O_5, TiO_2, or ZrO_2 nanocoating layers could be formed by dipping ZnO films into metal alkoxide solutions of low concentrations and subsequent heat treatments. The performance of DSSCs using the coated ZnO electrodes depends strongly on the structure of coating layers such as the thickness and the surface coverage, which are significantly influenced by the coating conditions. In particular, SiO_2 and Nb_2O_5 coating layers are effective to suppress the recombination by constructing the energy barrier at the ZnO/electrolyte interface and enhance energy conversion efficiency. It is found that the coating layers also hinder the grain growth of ZnO, contributing to the enhanced cell performance as well.

1. Introduction

Conventional photovoltaic devices are based on light harvesting and charge separation at semiconductor p-n junctions. In contrast, dye-sensitized solar cells (DSSCs) utilize a combination of wide-gap semiconductors and organic or metal-organic complex dyes which play a fundamental role in light harvesting. DSSCs are expected as one of the promising candidates to partially replace conventional silicon-based solar cells because of their low manufacturing cost and higher conversion efficiency over 10% [1]. Furthermore, since DSSCs are also applicable to colorful, lightweight, and flexible devices, they can be installed in many kinds of places. Common DSSCs are composed of a conductive transparent glass substrate, a metal oxide layer, dye-sensitizers chemically bonded to metal oxides, a liquid electrolyte, and a counter electrode. In particular, an assembly of the conductive transparent glass substrate and the dye-sensitized n-type metal oxide semiconductor layer is called a photoanode, which is an essential part of DSSCs.

TiO_2 is recognized as the most common electrode material for DSSCs because the TiO_2-based cells generally have higher-energy conversion efficiencies. Many kinds of metal oxide semiconductors other than TiO_2 have also been applied to electrodes of DSSCs [5]. Among them, ZnO is the most promising alternative to TiO_2. Many researchers have tried to enhance the performance of ZnO-based DSSCs by modifying nanostructures of electrodes. For example, Law et al. reported the energy conversion efficiency (η) of 1.5% for a ZnO nanowire electrode [6]. Keis et al. reported porous ZnO electrodes fabricated by a doctor blading method showing $\eta = 5\%$ under lower irradiance at 0.1 sun [7]. Other structures have been reported later such as ZnO aggregate films comprising of closely packed nanocrystallites ($\eta = 5.4\%$, 1 sun), densely packed nanosheet ZnO films ($\eta = 5.41\%$, 1 sun), and ZnO nanoparticles-nanowire hybrid arrays ($\eta = 4.24\%$, 1 sun) [8–10]. A more complicated structure of hierarchical ZnO nanowire electrodes showed the η of 2.63% [11]. We have also focused on ZnO as an electrode material in our series of studies on DSSCs [12–18]. Wurtzite-type ZnO is an *n*-type semiconductor with a wide band gap of 3.37 eV [19], which is similar to that of TiO_2 (3.2–3.3 eV) [20]. A conduction band edge energy (E_{CB}) of ZnO is located just above an E_{CB} of TiO_2, and a difference in

E_{CB} is within 200 meV between ZnO and TiO_2 [21–23]. In addition, ZnO has a high electron mobility by 10^7 times larger than that of TiO_2 when measured in bulk crystals [24]. Thus, a similar electron injection behavior can be expected for both materials, and ZnO is assumed to be more advantageous in terms of transport of the injected electrons. In spite of these excellent properties of ZnO, energy conversion efficiencies of ZnO-based DSSCs are still lower than those of TiO_2-based DSSCs. One of the reasons is lower open-circuit voltage (V_{OC}) of ZnO-based cells (typically 0.55–0.65 V) compared to that of TiO_2-based cells (0.75–0.85 V) when using Ru(II) complex sensitizers [1, 8, 16]. It is reported that a maximal V_{OC} is determined by an energy difference between E_{CB} of a semiconductor layer and the Nernst potential of an electrolyte [1, 5]. Therefore, ZnO-based DSSCs are potentially comparable to TiO_2-based cells in V_{OC} taking account of the large similarity in the band structure.

The difference in V_{OC} is due possibly to a recombination, namely, capturing photogenerated electrons in the conduction band of metal oxide semiconductor layers by oxidized species in an electrolyte. In an I^-/I_3^- redox system, tri-iodide ions (I_3^-) can be related to the recombination. The relationship between V_{OC} and a recombination kinetic constant (k_b) is represented by the following equation [25]:

$$V_{OC} = \left(\frac{kT}{e}\right) \ln\left(\frac{I_{inj}}{n_{cb} k_b [I_3^-]}\right), \quad (1)$$

where k is the Boltzmann constant, T is temperature, e is the electron charge, I_{inj} is the flux of injections, n_{cb} is the number of electrons in a conduction band, and $[I_3^-]$ is a concentration of tri-iodide ions in an electrolyte. Equation (1) implies that the larger recombination rate constant leads to the lower V_{OC} values. Therefore, the recombination should be suppressed to improve the V_{OC} values.

Some strategies have been conceived to suppress the recombination: (i) reducing the number of recombination sites, (ii) enhancing the electron transport inside electrodes, and (iii) constructing an energy barrier at an electrode/electrolyte interface. In ZnO electrodes, since the recombination sites correspond mainly to surface defects of ZnO particles, V_{OC} is supposed to be improved by decreasing surface areas of ZnO electrodes. A better electron transport is expected for the structure free from grain boundaries such as nanorods, nanowires, and nanorod/nanoparticle composite, which are also effective for enhancing V_{OC} [6, 26]. However, these ways (i) and (ii) are accompanied with a remarkable decrease in surface areas of electrodes, thereby resulting in a poor dye adsorption ability.

In the third way (iii), a formation of core-shell-type nanocoating layers, which act as an energy barrier for the recombination, on ZnO particles can reduce effectively the recombination kinetics constant k_b [27]. A schematic energy diagram for the DSSC using an insulator-coated ZnO electrode is shown in Figure 1 with an illustration of an ideal coating layer structure. The difference in E_{CB} between ZnO and proper coating materials can work as an energy barrier for the recombination at the ZnO/electrolyte interface. However, when E_{CB} of the coating material lies above the excited state of dye (S^*), the coating layer also disturbs the electron injection from adsorbed dyes into the ZnO layer. Nonetheless, many works are found in the literature reporting that insulator-coated electrodes are utilized to enhance the cell performance by the suppression of the recombination [28, 29]. Some researchers explain that the electron injection through ultrathin coatings of insulator electrodes is achieved by a tunneling effect [29, 30]. In fact, the performance comparable to the TiO_2 electrodes was reported for SnO_2/ZnO electrodes [31].

In addition to the suppression of the recombination, metal-oxide coatings may be suitable for inhibiting aggregation of Zn^{2+}/Ru(II) dye complexes or improving a long-term durability. For metal oxide nanocoatings on porous ZnO electrodes, we employed a dip-coating method using various kinds of metal alkoxide solutions. The coating solutions penetrate inside porous, thick ZnO films as electrodes. Then thin metal-oxide coatings are formed on the surface of ZnO particles by a sol-gel transformation including hydrolysis and condensation of the metal alkoxides as follows [32]:

$$M(OR)_m + nH_2O \longrightarrow M(OR)_{m-n}(OH)_n + n\text{ROH} \quad (2)$$

$$\text{M–OH} + \text{HO–M} \longrightarrow \text{M–O–M} + H_2O \quad (3)$$

In this paper, we review our works for enhancing the performance of DSSCs by the formation of SiO_2 and Nb_2O_5 nanocoating layers on ZnO electrodes [2, 3]. Additionally, we also report our recent works for the application of TiO_2 and ZrO_2 nanocoatings to the ZnO-based DSSCs.

2. Experimental

2.1. Fabrication of Porous ZnO Films. Porous, thick ZnO films used as a coating target were fabricated by a chemical bath deposition (CBD) method and subsequent pyrolytic transformation. Details of the fabrication process were reported previously [14]. Zinc acetate dihydrate ($(CH_3COO)_2Zn\cdot 2H_2O$; 99.0% purity, Wako Pure Chemical Industries Co., Ltd., Japan) was dissolved in dehydrated methanol at a concentration of 0.15 M. Fluorine-doped tin-oxide-coated glass substrates (FTO substrates; Nippon Sheet Glass Co., Ltd., Japan; sheet resistance of 10 ohm sq^{-1}) were immersed in the resultant solution, which was kept at 60°C for 30 h. Layered hydroxide zinc acetate (LHZA) films were formed on both sides of the FTO substrates. The unnecessary film on the bare glass side was completely removed by scratching. The film on the FTO substrate was heated at 450°C for 10 min in air to be converted to the porous, thick ZnO film (designated as the "uncoated" film).

2.2. Metal-Oxide Coating Method. Nanocoating layers were formed on the porous ZnO films through a dip-coating procedure. Four kinds of metal oxides were chosen as coating materials: SiO_2, Nb_2O_5, TiO_2, and ZrO_2. Metal alkoxide solutions were used for precursors. For the SiO_2 coating, a coating solution was prepared from 40 μL of tetraethylorthosilicate (TEOS; $(C_2H_5O)_4Si$; 95.0% purity, Wako), 500 μL of aqueous ammonia (28% mass/mass; Wako), and 20 mL

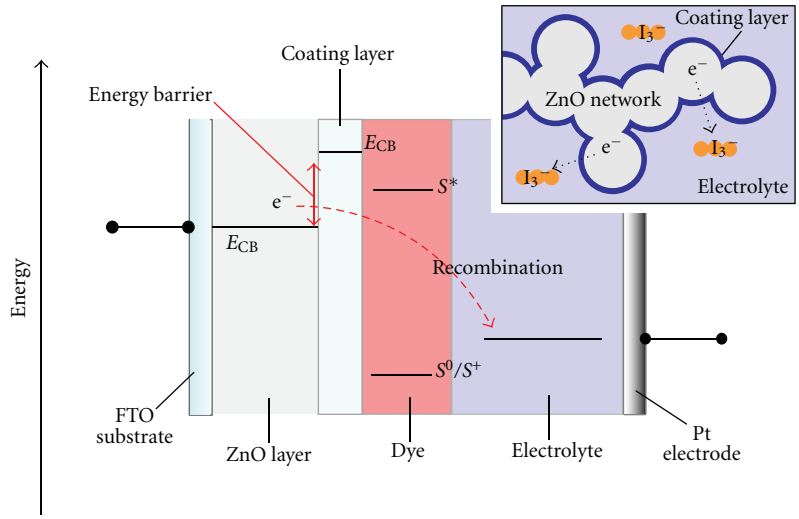

Figure 1: A schematic illustration of the suppression of the recombination by constructing an energy barrier at the ZnO/electrolyte interface. An inset indicates the core-shell-type coating layer on the ZnO electrode.

of water [33]. For the Nb_2O_5 coating, 10–30 mM ethanolic solutions of niobium pentaethoxide ($(C_2H_5O)_5Nb$; 99.9% purity, Soekawa Chemicals Co., Ltd., Japan) were prepared as coating solutions. For the TiO_2 and the ZrO_2 coating, 10–30 mM ethanolic solutions of titanium tetraisopropoxide ($[(CH_3)_2CHO]_4Ti$; 95.0% purity, Wako) and 10–50 mM 1-propanolic solutions of zirconium tetra-*n*-propoxide ($(C_3H_7O)_4Zr$; 23–28% free alcohol, Strem Chemicals, Inc., USA) were prepared as coating solutions, respectively. The ZnO films were immersed in the respective coating solutions and withdrawn at a speed of 0.1 mm/sec by using a Micro Speed Dip Coater (MS215, Asumi Giken Ltd., Japan). Then, the coated ZnO films were heated at 600°C for 10 min in air. We also prepared a reference sample by heating the uncoated ZnO film at 600°C for 10 min (the "uncoated/heated" film).

2.3. Characterization. The crystal structure was identified by X-ray diffraction (XRD) analysis (Bruker, AXS D8-02) using CuKα radiation. The Scherrer diameter of particles constituting the sample films was calculated with the Scherrer equation from the recorded XRD data. The morphology of the sample films was observed by field-emission scanning electron microscopy (FESEM; Hitachi, S-4700). The structure of the metal-oxide coating layers was examined by field-emission transmission electron microscopy (FETEM; FEI, Sirion or Tecnai Spirit) and X-ray photoelectron spectroscopy (XPS; JEOL, JPS 9000 MX).

2.4. Evaluation of Cell Performance. The uncoated and the coated ZnO films were dyed by immersion in a 0.3 mM ethanolic solution of $RuL_2(NCS)_2$: 2TBA (L = 2,2′-bipyridyl-4,4′-dicarboxylic acid and TBA = tetrabutylammonium; N719, Solaronix SA, Switzerland) at 60°C for 30 min. For *J-V* measurements, sandwich-type open cells were constructed with the ZnO/N719 photoanode, a 50 μm-thick spacer film, and a counter platinum electrode. The I^-/I_3^- redox couple electrolyte, which was composed of 0.1 M LiI, 50 mM I2, 0.6 M 1,2-dimethyl-3-propylimidazolium iodide, 1 M 4-tert-butylpyridine, and 3-methoxypropionitrile, was introduced between the electrodes. The characteristic values, V_{OC}, short-circuit photocurrent density (J_{SC}), fill factor (ff), and η, were determined from the *J-V* measurements. The active cell area was fixed at 25 mm^2 by a mask. A 500 W Xe lamp (Ushio, UXL-500SX) was used as the light source to produce the simulated AM 1.5 illumination at 100 mW/cm^2. An AM 1.5 filter, a water filter, and an infrared cut filter (Hoya, S76-HA50) were placed in the light path to regulate light in the wavelength range of 300–800 nm, reducing the mismatch of the simulated sunlight. *J-V* curves were measured under the simulated sunlight with a potentiostat (Hokuto Denko, HSV-100).

The amount of dyes adsorbed on the electrodes was estimated by removing them in a 0.5 M NaOH ethanol/water ($v/v = 1$) solution. The absorbance of the resultant dye solutions was measured by a spectrophotometer (Hitachi, U-3300 or Jasco, V-670) and calibrated with a standard solution of N719.

3. Results and Discussion

3.1. Structure of SiO_2- and Nb_2O_5-Coated ZnO Films. The film obtained by the CBD method was identified as LHZA with the chemical formula of $Zn_5(OH)_8(CH_3COO)_2 \cdot 2H_2O$. They had a unique flower-like morphology. The LHZA film could be converted into ZnO completely by pyrolysis at 450°C for 10 min. An FESEM image of the resultant ZnO film is shown in Figure 2(a), where the flower-like morphology originated from the LHZA film is maintained well. There exist micrometer-sized spaces inside as well as between the flower-like ZnO units, which can facilitate the penetration of the coating solutions in the coating process, the dye loading during the immersion in the dye solution, and the diffusion of the electrolyte in the solar-cell operation.

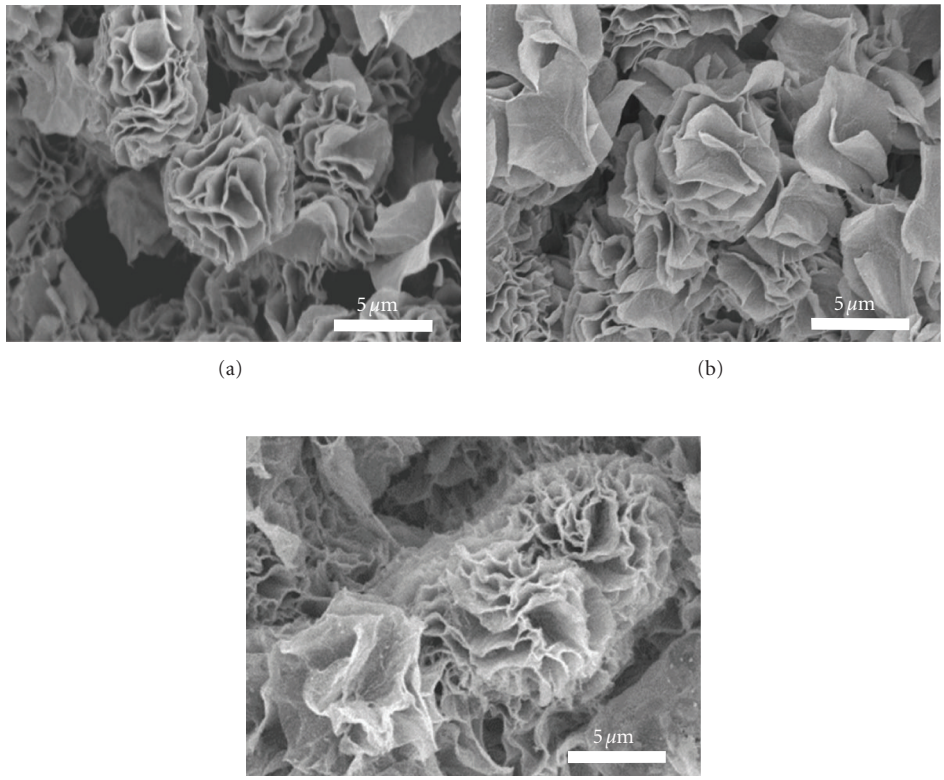

(a) (b) (c)

Figure 2: FESEM images of (a) the uncoated ZnO, (b) the SiO_2-coated ZnO, and (c) the Nb_2O_5 (10 mM)-coated ZnO film [2–4].

Figures 2(b) and 2(c) show FESEM images of the films that were coated with the TEOS solution and the 10 mM $(C_2H_5O)_5Nb$ solution, respectively, and subsequently heated at 600°C for 10 min (denoted as the "SiO_2-coated" and the "Nb_2O_5 (10 mM)-coated" film, resp.). The flower-like morphology of the ZnO film does not change after the SiO_2 and the Nb_2O_5 coating. The thickness of the coated films (approximately 30 μm) was also the same as that of the ZnO film. Therefore, it is not necessary to consider influences of dissolution or morphological change in discussing the structure and properties of the coated ZnO films.

The presence of the coating materials was confirmed by XPS. Figure 3(a) compares XPS spectra in the Si 2p region for the uncoated and the SiO_2-coated ZnO film. While no peak is detected for the uncoated ZnO film in this region, a peak due to the Si 2p electrons is clearly observed at 102.0 eV for the SiO_2-coated ZnO film, supporting the presence of SiO_2 in the coated film. We also tried to observe directly the SiO_2 coating layers by FETEM. Figure 4 shows an FETEM image of the SiO_2-coated ZnO particles found in the film. The core-shell-type SiO_2 coating layers with a thickness of 1–3 nm are formed on the surface of the ZnO particles. We have reported previously that the structure of the silica layers, such as the thickness and the surface coverage, depends on the TEOS concentration and the coating time [4]. Basically, in the presence of the diluted ammonia catalyst, the formation of an amorphous SiO_2 layer proceeds as the following hydrolysis and condensation reactions [32]:

$$\mathrm{Si(OC_2H_5)_4} + n\mathrm{OH^-} \longrightarrow \mathrm{Si(OC_2H_5)_{4-}}_n\mathrm{(O^-)}_n + n\mathrm{C_2H_5OH} \quad (4)$$

$$\equiv\mathrm{Si{-}OH} + \mathrm{O^-{-}Si} \equiv \longrightarrow \equiv\mathrm{Si{-}O{-}Si} \equiv + \mathrm{OH^-} \quad (5)$$

Because of the lower stability of TEOS in the aqueous system, the reactions might proceed rapidly. Then the core-shell structure is formed by the reaction between the surface OH groups of the ZnO particles and the hydrolyzed TEOS. Actually, the thin SiO_2 nanocoating layers were successfully formed by using the low TEOS concentration of approximately 9 mM and the relatively short coating time (the ZnO film was immersed in the coating solution only for a few minutes). It should be noted that the thin shell layers could cover partially the surface of the ZnO particles in such the condition.

The SiO_2 coating layers were in the amorphous state regardless of the subsequent heat treatments. In contrast, for the crystalline metal oxide coatings, it is important to know crystalline phases formed in the sol-gel transformation under the given experimental conditions. Since niobium is a multivalent metal element, there are various stoichiometries found in niobium oxides, Nb_xO_y. Moreover, as far as Nb_2O_5

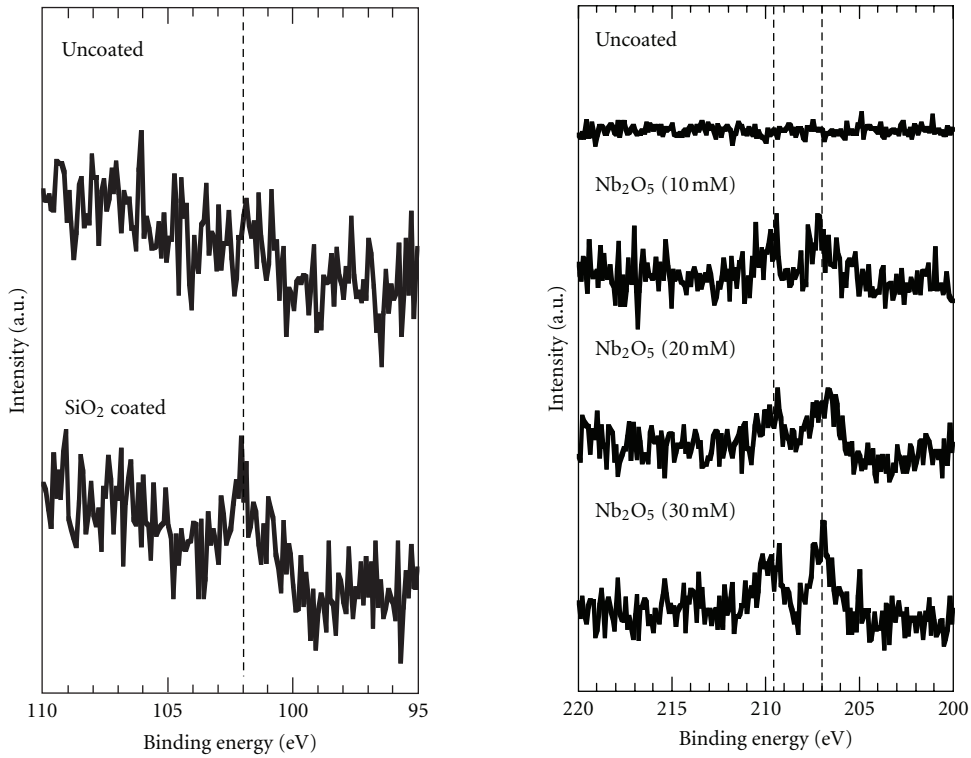

Figure 3: XPS spectra (a) in the Si 2p region for the uncoated and the SiO_2-coated electrodes and (b) in the Nb 3d region for the uncoated and the Nb_2O_5-coated electrodes [2, 3].

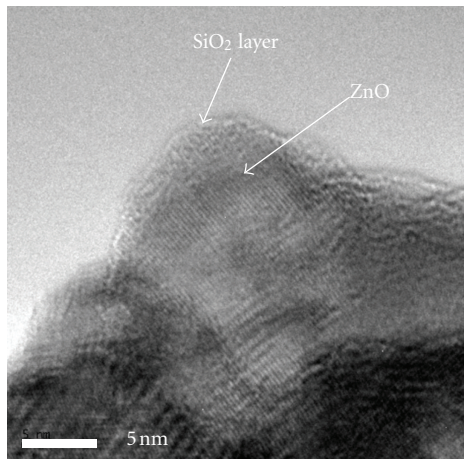

Figure 4: An FETEM image of the SiO_2-coated ZnO particles [2].

is concerned, at least 12 types of crystal structures are known [34]. In our case [3], the Nb_2O_5 coating layer derived from the $(C_2H_5O)_5Nb$ solution was supposed to be the TT phase which could be classified as the quasi-hexagonal crystal system. Figure 3(b) compares XPS spectra in the Nb 3d region for the uncoated and the Nb_2O_5-coated ZnO films. No peak is seen for the uncoated ZnO film, whereas the Nb $3d_{3/2}$ and $3d_{5/2}$ peaks appear at 209.5 and 207.0 eV, respectively, for all the Nb_2O_5-coated ZnO films. The presence of niobium in the films is, thus, confirmed and the formation of the Nb_2O_5 coating layer is supported. Unfortunately, the Nb_2O_5 coating layers could not be observed directly by FETEM because the ZnO particles were decomposed by an electron beam accelerated at high voltage. In turn, an additional effect of the coatings was found in the TEM observation. Figure 5(a) shows a TEM image of the ZnO particles of the uncoated film which was used as the coating target. ZnO nanoparticles around 20 nm in size are clearly observed. When the uncoated ZnO film is heated at 600°C for 10 min, the growth of the ZnO particles was promoted and the particle size was increased up to more than 50 nm (Figure 5(b)). On the other hand, the growth of both the SiO_2- and the Nb_2O_5-coated ZnO particles is hindered even after heating at 600°C, and the particle size is kept around 20 nm (Figures 5(c)–5(f)). These results imply that the nanocoating layers actually exist on the surface of the ZnO particles and disturb the mass transport related to the grain growth or sintering during heating. Accordingly, the SiO_2 and the Nb_2O_5 nanocoatings are successfully formed on the ZnO electrodes. In the XRD analysis, diffraction peaks due to ZnO did not show any shift after the SiO_2 and Nb_2O_5 coating process, indicating that the lattice strain due to doping or stress was negligible for discussing the coating effect.

3.2. Structure of TiO_2- and ZrO_2-Coated ZnO Films. To know crystal phases of TiO_2 and ZrO_2 coating layers, we characterized first as-prepared and heat-treated gels which were

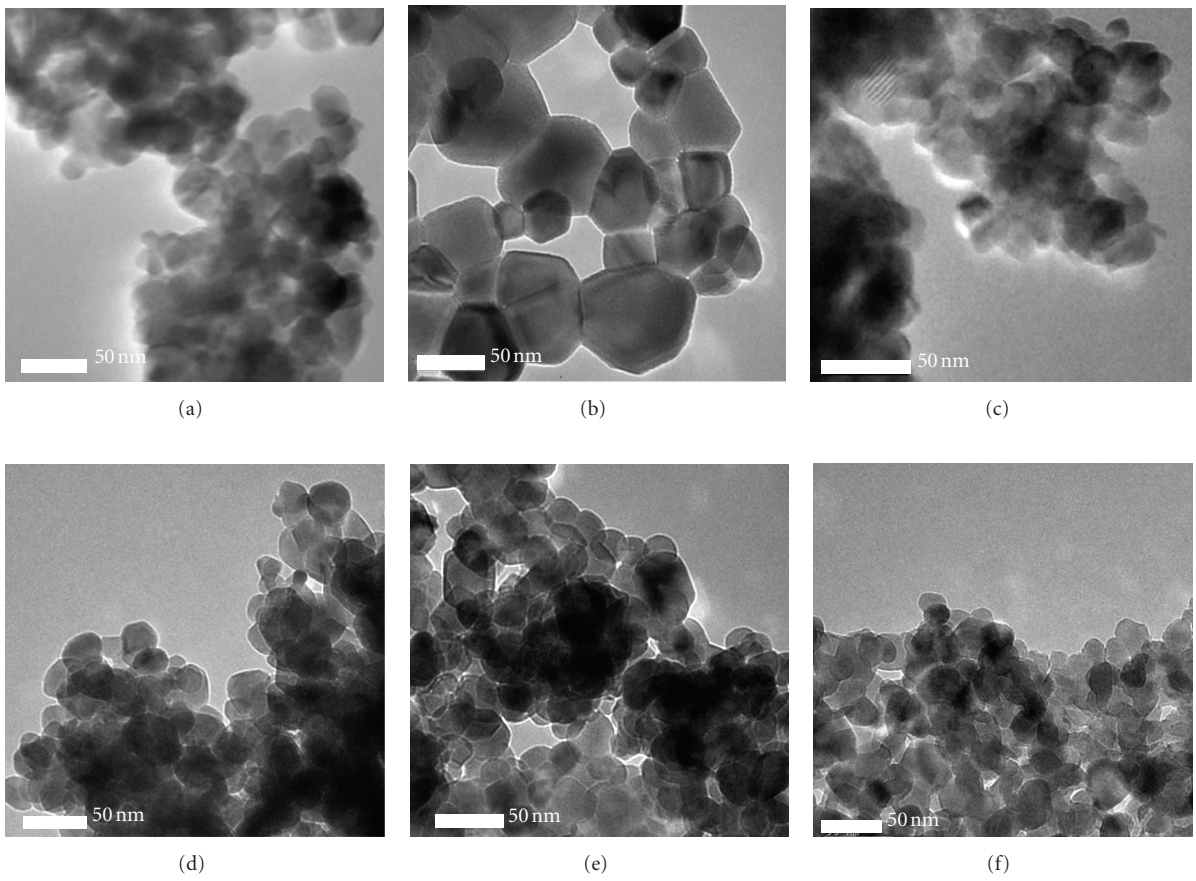

Figure 5: FETEM images of (a) the uncoated, (b) the uncoated/heated, (c) the SiO_2-coated films, and the films coated with (d) 10 mM, (e) 20 mM, and (f) 30 mM of the $(C_2H_5O)_5Nb$ solutions [2, 3].

obtained by forced hydrolysis of $[(CH_3)_2CHO]_4Ti$ in ethanol and $(C_3H_7O)_4Zr$ in 1-propanol by adding water. XRD patterns of the as-prepared and the heated titanium oxide gels are shown in Figure 6(a). The as-prepared titanium oxide gel is amorphous, whereas the gel heated at 600°C is a mixture of anatase and brookite phases of TiO_2. The as-prepared zirconium oxide gel is also amorphous, and a crystalline phase is observed for the gel heated at 600°C (Figure 6(b)) with XRD peaks originating from tetragonal or cubic ZrO_2. The heated gel was further analyzed by Fourier transform infrared (FT-IR) spectroscopy (data not shown). The result showed that a band related to the tetragonal ZrO_2 was detected at 575 cm^{-1} [35]. Therefore, the TiO_2 and the ZrO_2 coating layers, as described below, are regarded as the mixture of anatase- and brookite-type TiO_2 and the tetragonal ZrO_2, respectively.

For the TiO_2- and the ZrO_2 coated ZnO films, the morphology and the thickness did not change after the coating procedures including subsequent heating. The coated films were examined by XPS to confirm the presence of the TiO_2 and the ZrO_2 coating layers. Figure 7(a) compares XPS spectra of the uncoated and the TiO_2-coated ZnO films. For the TiO_2 (20 mM)-coated and the TiO_2 (30 mM)-coated ZnO film, a Ti $2p_{1/2}$ peak can be observed at 458.6 eV. Figure 7(b) compares XPS spectra of the uncoated and the ZrO_2-coated ZnO films. While no peak is seen for the uncoated ZnO film, two peaks appear in all the spectra for the coated films at approximately 184.4 eV and 182.0 eV, corresponding to the binding energy of Zr $3d_{3/2}$ and $3d_{5/2}$ electrons, respectively. The XPS results suggest that the ZrO_2-coating layers are formed on the ZnO particles regardless of the $(C_3H_7O)_4Zr$ concentration, whereas the TiO_2 coating layers are formed at least in the TiO_2 (20 mM)-coated and the TiO_2 (30 mM)-coated film.

The formation of the TiO_2 and the ZrO_2 coating layers could not be observed by FETEM, for the same reason as mentioned above. Then we tried to see the hindrance of the grain growth. Low magnification TEM images of the TiO_2- and the ZrO_2-coated ZnO films is shown in Figure 8. Compared to the uncoated/heated ZnO particles shown in Figure 5(b), the size of the TiO_2- and the ZrO_2-coated ZnO particles are smaller, indicative of the hindrance effect. The TiO_2 and the ZrO_2 coating layers are then suggested to be formed on the ZnO particles, as in the case of the SiO_2 and the Nb_2O_5 coating.

It should be noted that the size of the TiO_2- and the ZrO_2-coated ZnO particles appears to be slightly larger than that of the SiO_2- and the Nb_2O_5-coated particles. The

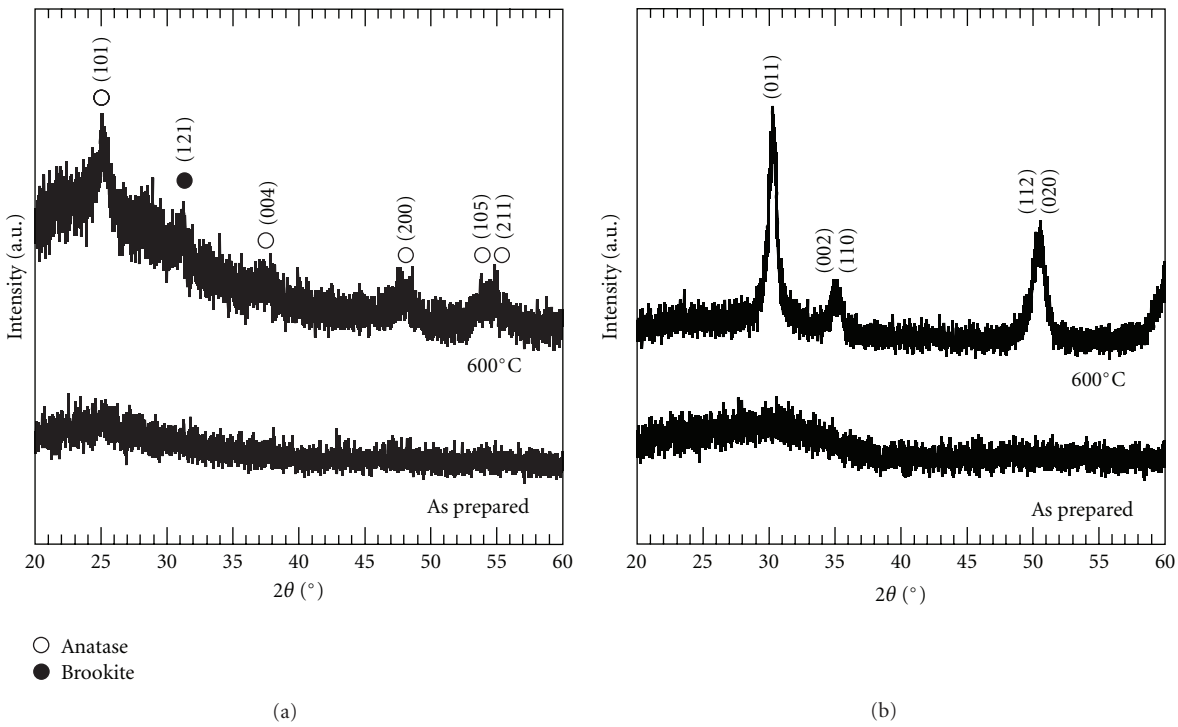

Figure 6: XRD patterns of (a) the as-prepared and the heated titanium oxide gel and (b) the as-prepared and the heated zirconium oxide gel.

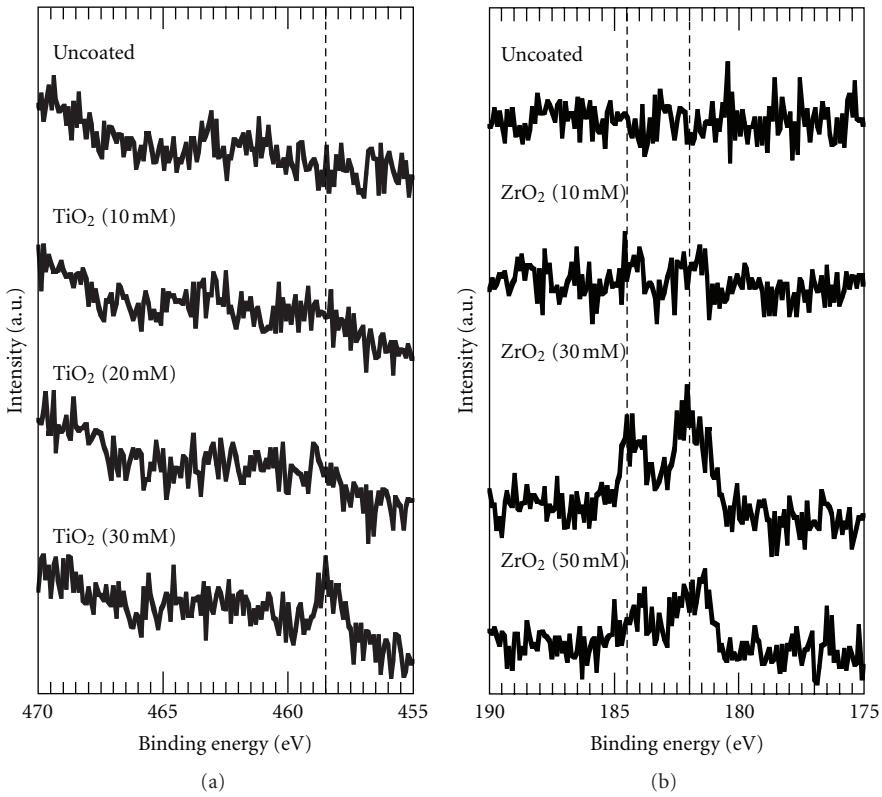

Figure 7: XPS spectra (a) in the Ti 2p region for the uncoated and the TiO_2-coated electrodes and (b) in the Zr 3d region for the uncoated and the ZrO_2-coated electrodes.

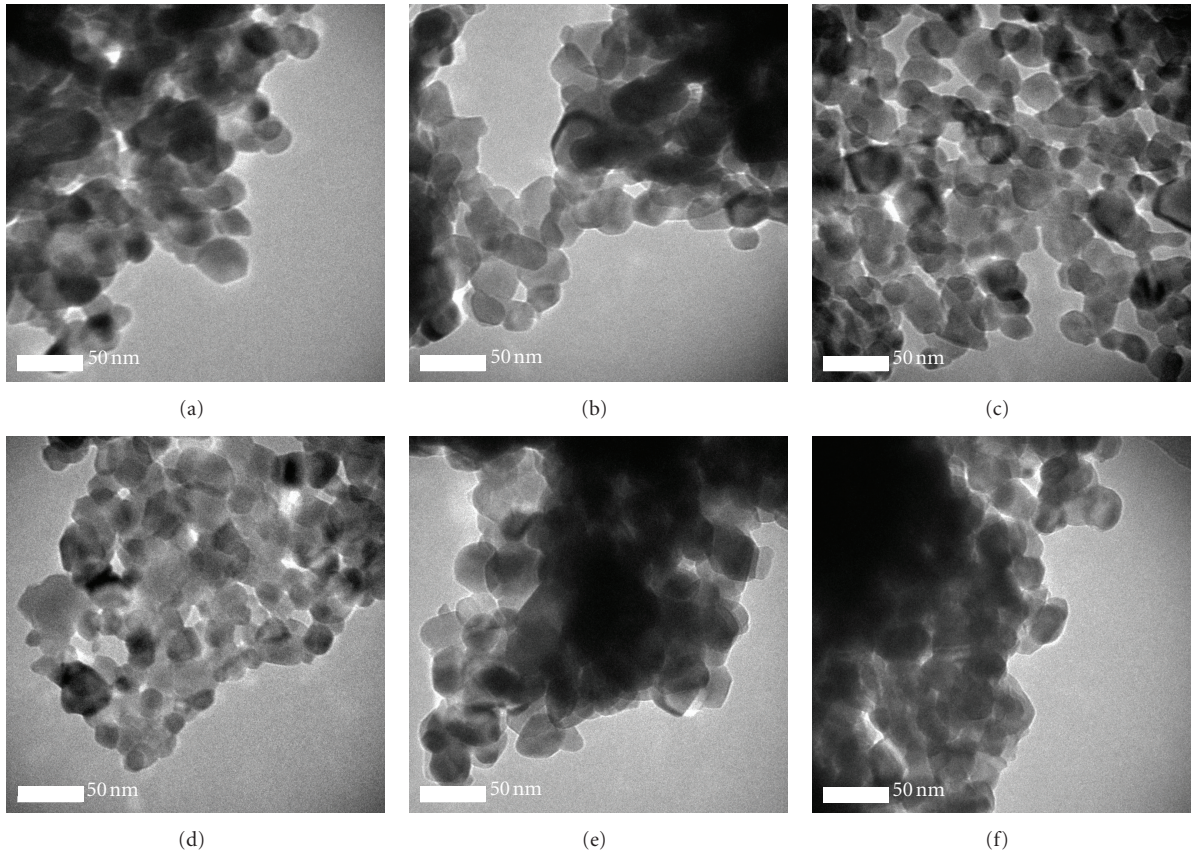

Figure 8: FETEM images of the films coated with (a) 10 mM, (b) 20 mM, and (c) 30 mM of the $[(CH_3)_2CHO]_4Ti$ solutions and the films coated with (d) 10 mM, (e) 30 mM, and (f) 50 mM of the $(C_3H_7O)_4Zr$ solutions.

Scherrer diameter of the uncoated and all the coated ZnO films was evaluated quantitatively from the XRD data by using the following Scherrer equation [36]:

$$D = \frac{0.9\lambda}{\beta \cos\theta}, \tag{6}$$

where λ is the wavelength of the X-ray irradiation (CuKα = 1.5418 Å), β is the full width of half maximum (FWHM) of the peak, and θ is the diffraction angle. Figure 9 compares the Scherrer diameters calculated for the (100), (002), and (101) peaks of ZnO. In Figure 9(a), the Scherrer diameters of the SiO_2- and the Nb_2O_5-coated ZnO particles are approximately the same as that of the uncoated ZnO (around 21 nm). In contrast, for the uncoated/heated ZnO, the Scherrer diameter increases up to 35 nm due to the grain growth by heating. The TiO_2- and the ZrO_2-coated ZnO particles show the larger diameters than that of the uncoated ZnO particles (Figure 9(b)), indicating that the hindrance of the grain growth is less effective for the TiO_2 and the ZrO_2 coating. There are two possible reasons for such the difference between the coating materials. Firstly, the ability to suppress the grain growth of ZnO may be peculiar for a certain kind of metal oxides. Secondly, the surface coverage of the coating layers formed by the sol-gel transformation is different among the respective metal oxides. The hindrance of the ZnO grain growth arises from disturbing the mass transportation by the coating layers, which means that the latter reason is more probable. That is, the coating layers on the ZnO particles with the lower surface coverage allow the grain growth to occur more rapidly by heating. Actually, the Scherrer diameter of the TiO_2- and the ZrO_2-coated ZnO decreases with the concentration of the metal alkoxides in the coating solutions (Figure 9(b)). This fact is consistent with the basics of the dip-coating method; the thickness and the surface coverage of the coating layers depend directly on the concentration of the metal source. The XPS results also suggested the lower surface coverage for the films coated with the lower concentration of the coating solutions. Hence, we tentatively conclude that the increase in the Scherrer diameter for the TiO_2- and the ZrO_2-coated ZnO particles is attributed to the lower surface coverage of the coating layers, which might be influenced by the kinetics of the sol-gel transformation. Additionally, the lattice strain of ZnO due to doping or stress was not found by the coating process as in the case for the SiO_2 and Nb_2O_5 coating.

3.3. Performance of DSSCs using the Coated Electrodes. The cell performance of DSSCs using the uncoated and the coated ZnO electrodes was evaluated from the *J-V* measurements. The characteristic values, V_{OC}, J_{SC}, ff, and η, together with the amount of the adsorbed dye, are summarized in Table 1. *J-V* curves of the uncoated, the uncoated/heated, and the

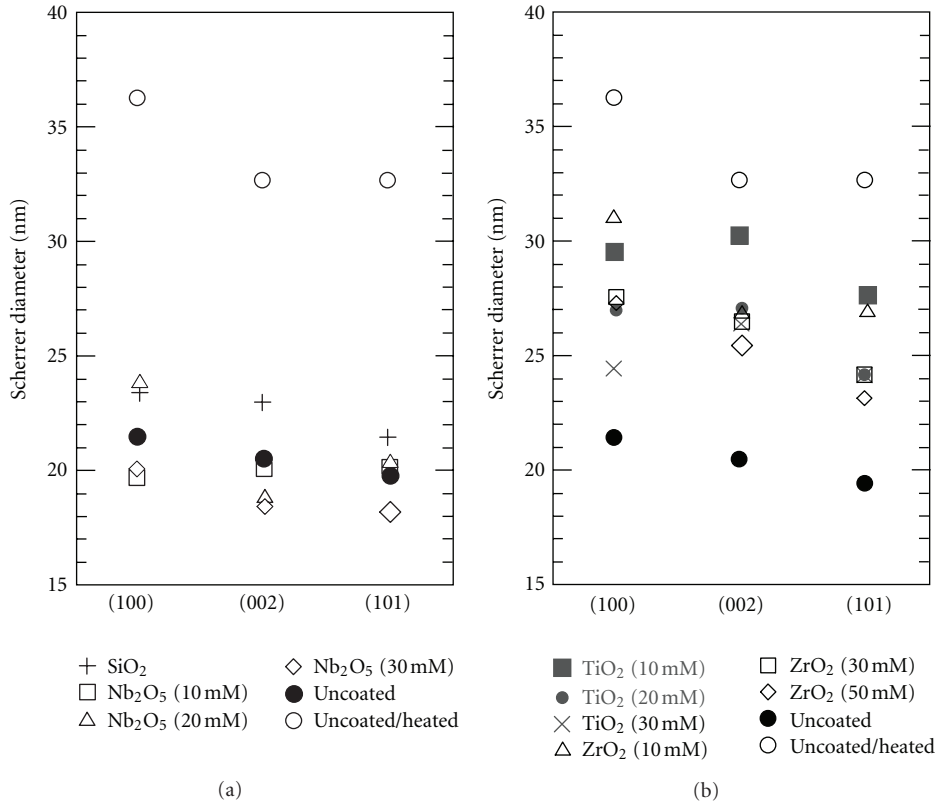

Figure 9: The Scherrer diameters for (a) the SiO_2- and the Nb_2O_5-coated and (b) the TiO_2- and the ZrO_2-coated ZnO films with respect to the (100), (002), and (101) planes of ZnO.

Table 1: The cell performance of the DSSCs using the uncoated and the coated ZnO electrodes [2, 3].

Electrode	V_{OC} (V)	J_{SC} (mA cm^{-2})	ff (−)	η (%)	Dye adsorption (10^{-7} mol cm^{-2})
Uncoated	0.683	11.59	0.578	4.57	1.08
Uncoated/heated	0.718	7.11	0.535	2.73	0.55
SiO_2 coated	0.724	12.05	0.550	4.80	0.89
Nb_2O_5 (10 mM) coated	0.712	12.42	0.587	5.19	0.76
Nb_2O_5 (20 mM) coated	0.741	10.67	0.549	4.34	1.12
Nb_2O_5 (30 mM) coated	0.755	9.43	0.577	4.10	1.02
TiO_2 (10 mM) coated	0.729	9.18	0.503	3.37	0.92
TiO_2 (20 mM) coated	0.730	10.01	0.512	3.74	0.92
TiO_2 (30 mM) coated	0.730	9.54	0.501	3.49	0.88
ZrO_2 (10 mM) coated	0.765	7.71	0.570	3.36	1.01
ZrO_2 (30 mM) coated	0.746	9.53	0.545	3.87	1.09
ZrO_2 (50 mM) coated	0.746	9.16	0.551	3.77	0.94

SiO_2-coated ZnO electrodes are shown in Figure 10(a). Firstly, the cell performance of the DSSCs using the uncoated and the uncoated/heated electrodes is discussed. The cell using the uncoated ZnO electrode shows V_{OC} of 0.683 V, J_{SC} of 11.59 mA/cm^2, and conversion efficiency of 4.57%. In the cell using the uncoated/heated electrode, V_{OC} increases to 0.718 V while J_{SC} decreases to 7.11 mA/cm^2. These changes can be explained with the progress of the grain growth during heating [37]. The size of the ZnO particles heated at 600°C for 10 min increases up to more than 50 nm, leading to the significant decrease in the net surface area of the electrodes. Simultaneously, the recombination sites located at the surface of the ZnO particles are diminished by the high-temperature heating. Dark current-voltage curves shown in Figure 10(b) reveal that the dark current of the uncoated/heated electrode is much smaller than that of the uncoated electrode at the same bias. This fact also suggests that the recombination is strongly suppressed in

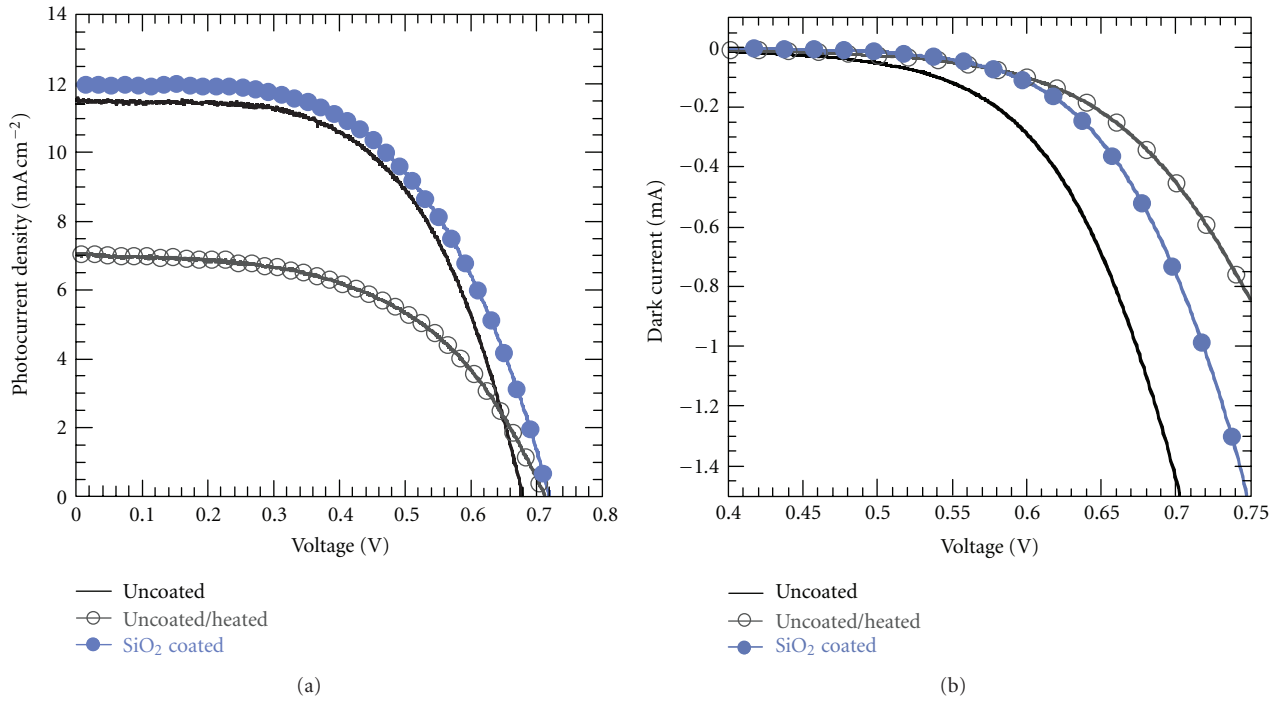

FIGURE 10: (a) *J-V* curves and (b) dark current-voltage curves of the cells using the uncoated, the uncoated/heated, and SiO_2-coated ZnO electrodes [2].

the uncoated/heated electrode. Hence, according to (1), the relatively high V_{OC} is obtained for the cell using the uncoated/heated electrode. On the other hand, the amount of the adsorbed dye decreases by half with the decrease in the surface area of the electrode, resulting in the significantly lowered J_{SC}. As a result, the energy conversion efficiency of the cells using the uncoated ZnO electrodes decreases from 4.57% to 2.73% by heating.

In the cell using the SiO_2-coated electrode, V_{OC} and J_{SC} increase to 0.724 V and 12.05 mA/cm^2, respectively, even after heating at 600°C [2]. The particle size does not change by heating due to the hindrance of the grain growth by the formation of the SiO_2 nanocoating layer on the ZnO particles. Therefore, the enhancement of the cell performance is attributed not to the decrease in the net surface area of the electrode but to the suppression of the recombination by constructing the energy barrier at the ZnO/electrolyte interface. The presence of the energy barrier is also suggested strongly by the smaller dark current of the SiO_2-coated electrode compared to that of the uncoated electrode at the same bias (Figure 10(b)). E_{CB} of SiO_2 is located at −0.20 eV versus E_{VAC}, which is approximately 4.0 eV above E_{CB} of ZnO, and this energy difference works as the barrier for the recombination [38]. Additionally, as the decrease in the surface area of the electrode can be avoided by the hindrance of the grain growth, the amount of the adsorbed dye for the SiO_2-coated electrode is comparable to that for the uncoated electrode. Both the suppression of the recombination and the hindrance of the grain growth by the SiO_2 coating layer contribute to the enhancement in J_{SC}. Due to the increase in V_{OC} and J_{SC}, the SiO_2-coated ZnO electrode exhibits higher-energy conversion efficiency of 4.80%. This result demonstrates that even the insulator coatings are effective to improve the cell performance including J_{SC}. Since E_{CB} of SiO_2 is located at higher energy level than the S^* state of N719 (approximately 3.65 eV above) [39], the electron injection may be retarded considerably. In the present case, the electron injection to the SiO_2-coated ZnO might be possible from the dye adsorbed on the "bare" ZnO surface rather than the tunneling effect because the thickness of the SiO_2 coating layer (1–3 nm) is too large.

Contrary to SiO_2, E_{CB} of Nb_2O_5 is located approximately 0.2 eV above E_{CB} of ZnO and 0.3 eV below the S^* state of N719 [39, 40]. Therefore, the Nb_2O_5-coating would not disturb the electron injection when they act as the energy barrier for the recombination [27]. *J-V* curves and dark current-voltage curves of the uncoated and the Nb_2O_5-coated ZnO electrodes are shown in Figure 11. As mentioned above, the hindrance effect of the grain growth is found in all the Nb_2O_5-coated electrodes. Higher V_{OC} for the Nb_2O_5-coated electrodes is then ascribed to the suppression of the recombination by the Nb_2O_5 coating layers. In addition, as can be seen in Figure 11(a) and Table 1, V_{OC} of the cells using the Nb_2O_5-coated ZnO electrodes increases from 0.712 to 0.755 V when the $(C_2H_5O)_5Nb$ concentration increases from 10 to 30 mM. This tendency of the V_{OC} increase may be due to the increase in the surface coverage of the Nb_2O_5 coating layers which work as the energy barrier for the recombination. In fact, as found in Figure 11(b), the dark current of the Nb_2O_5-coated electrodes decreases with the $(C_2H_5O)_5Nb$ concentration. Especially for the Nb_2O_5 (30 mM)-coated electrode, the dark current is as small as that

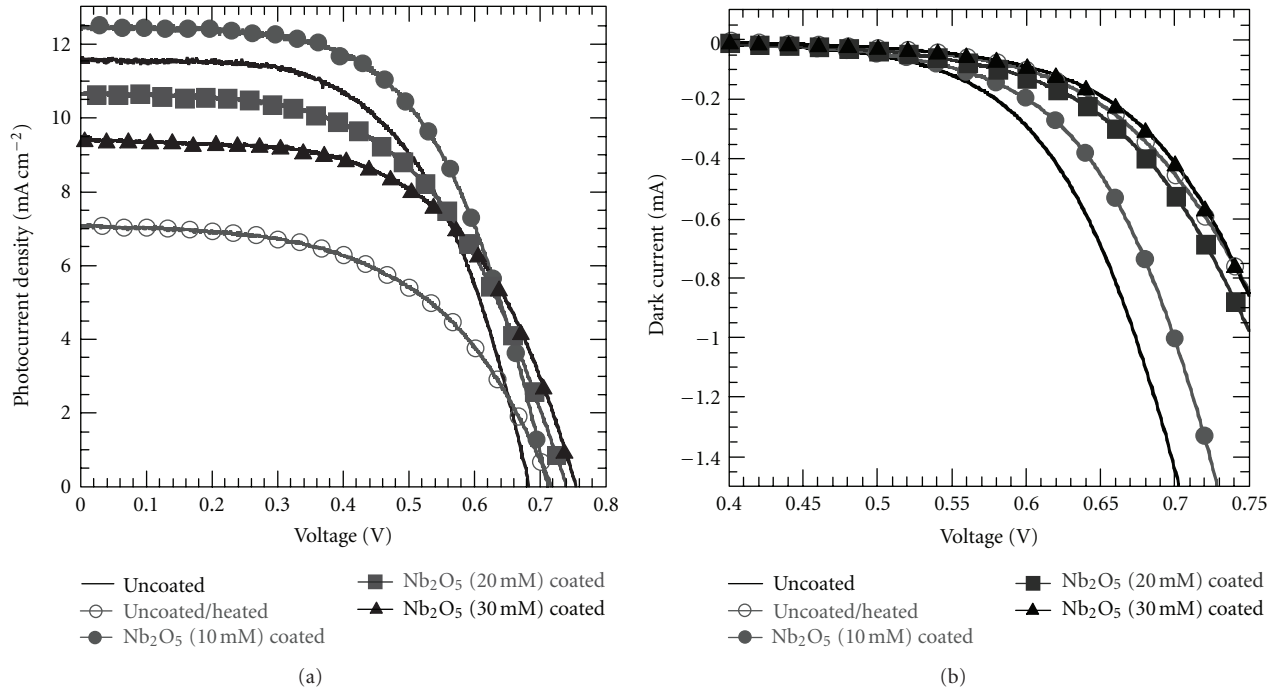

FIGURE 11: (a) *J-V* curves and (b) dark current-voltage curves of the cells using the uncoated, the uncoated/heated, and the Nb_2O_5-coated ZnO electrodes [3].

of the uncoated/heated electrode. This is probably because of the higher surface coverage of Nb_2O_5.

J_{SC} of the Nb_2O_5-coated electrodes, on the other hand, tends to decrease with the coating solution concentration. This is attributable to the lower electron conductivity of the Nb_2O_5 coating layers [34], judging from the fact that the dye adsorption ability is not changed by the coating. It is also reported that the charge injection efficiency from the Ru(II) complex dye to Nb_2O_5 is similar to that to ZnO [41]. The thicker coating layer with the higher coverage can possibly disturb the electron transport inside the electrode and decrease J_{SC} to some extent. For the Nb_2O_5 (10 mM)-coated ZnO electrode, since both V_{OC} and J_{SC} are improved due to the efficient suppression of the recombination and the hindrance of the grain growth, the higher energy conversion efficiency of 5.19% has been achieved. These results suggest that Nb_2O_5 is more suitable for coating on the ZnO electrodes than SiO_2.

In the case of the Nb_2O_5 coating, the ZnO particle size is kept constant (around 20 nm) regardless of the coating solution concentration. Only the structure of the coating layers is concerned. However, for the TiO_2 and the ZrO_2 coating, we need to consider both the structure of the coating layers and the influence of the grain growth. It is reported that E_{CB} of TiO_2 is approximately 0–200 meV below E_{CB} of ZnO, and hence the TiO_2 coating layers do not work as the energy barrier for the recombination. Actually, however, slight increase in V_{OC} is found in the cell using the TiO_2-coated ZnO electrodes. As shown in Figure 12(a), the dark current of all the TiO_2-coated electrodes is as small as that of the uncoated/heated ZnO electrode. According to Figure 9(b), the size of the TiO_2-coated ZnO particles slightly increases by heating, which contributes to the increase in V_{OC} by the reduction of the recombination sites. Considering that the TiO_2-coated ZnO particles are smaller than the uncoated/heated ZnO, the increased V_{OC} should be explained with the other factor than the grain growth. In other words, the TiO_2 coating layer is capable of acting as the energy barrier against our prediction. Actually, there are some reports on the successful TiO_2 coatings for improving the performance of DSSCs using ZnO electrodes [42, 43]. The enhancement in V_{OC} is ascribed to the passivation of the surface defects of the ZnO by TiO_2. As a result, the recombination from the ZnO layer is reduced [44]. Further investigations are necessary for TiO_2 to clarify the effect or the mechanism of the coating layers.

The decrease in the amount of the adsorbed dye results in the slightly smaller J_{SC} due to the decrease in the surface area by the slight grain growth of the TiO_2-coated ZnO particles. Additionally, the ff values for all the cells using TiO_2-coated ZnO electrode are remarkably smaller than those of the other electrodes. The decrease in ff is explained with a high intrinsic resistance of the cell [45]. In the present case, the electron transport may be disturbed through the TiO_2-coated ZnO particles inside the electrodes due to the small difference in E_{CB}.

ZrO_2 is also considered to work as the energy barrier. Similar to SiO_2, E_{CB} of ZrO_2 is located at −3.44 eV versus E_{VAC}, which is approximately 0.9 eV above E_{CB} of ZnO and 0.4 eV above the S^* state of N719 [38, 39]. The ZrO_2 (10 mM)-coated electrode exhibits the highest V_{OC} value of 0.765 V, which is comparable to that of the TiO_2-base

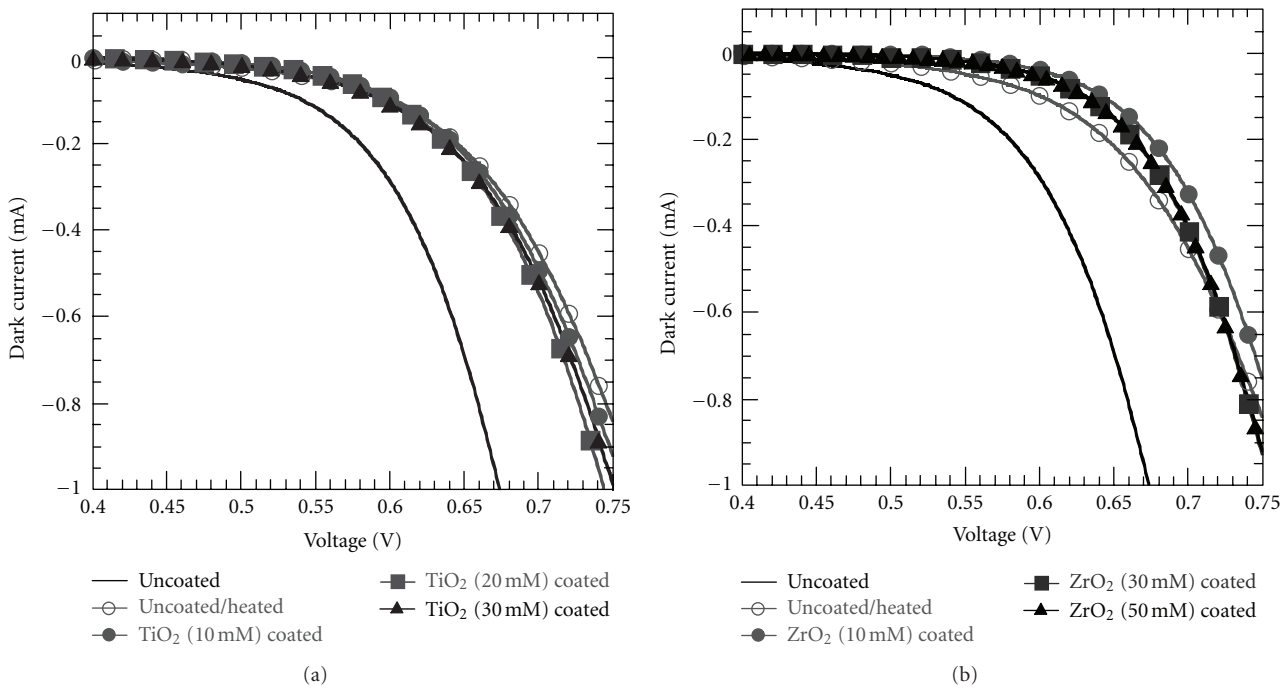

Figure 12: Dark current-voltage curves of the cells using (a) the uncoated, the uncoated/heated, and the TiO_2-coated ZnO electrodes and (b) the uncoated, the uncoated/heated, and the ZrO_2-coated ZnO electrodes.

DSSCs. The coverage of the ZrO_2 coating layer is considered to be small because the hindrance of the ZnO grain growth is less effective for the ZrO_2 coating (Figure 9(b)). In particular, the recorded dark current of the ZrO_2 (10 mM)-coated electrode is smaller than that of the uncoated/heated electrode (Figure 12(b)). This result also suggests that both the reduction of the surface recombination sites due to grain growth and the energy barrier constructed by the ZrO_2 coating contribute to the increase in V_{OC}. It is found that V_{OC} decreases when the ZnO electrodes are coated with 30 and 50 mM $(C_3H_7O)_4Zr$ solutions. This is because the influence of the decrease in the recombination sites on V_{OC} is diminished by the hindrance of the grain growth due to the higher coverage of the ZrO_2 coating. All the ZrO_2-coated electrodes show lower J_{SC} than that of the uncoated electrode. As the amount of the adsorbed dye does not change significantly after the ZrO_2 coating, the decrease in J_{SC} is due mainly to the interruption of the electron injection. As a result, the energy conversion efficiency of the cells slightly decreases by the ZrO_2 coating.

In this paper, the formation of metal-oxide nanocoatings on ZnO is demonstrated to be one of the promising approaches to the enhancement of the cell performance. Since V_{OC} of the cells using the coated ZnO electrodes depends both on the structure of the metal-oxide coating layers and the structure of the ZnO electrode itself, we should control carefully the sol-gel transformation conditions and the following heat treatments. We are now trying to form the ultrathin coating layers which suppress more effectively the recombination and enhance the performance of the ZnO-based DSSCs.

4. Conclusions

The nanoscale coating of four kinds of metal oxides (SiO_2, Nb_2O_5, TiO_2, and ZrO_2) were performed on the ZnO electrodes to increase V_{OC} of the DSSCs. Metal alkoxide solutions of low concentrations were employed to form nanocoating layers through the dip-coating method, followed by the sol-gel transformation. The SiO_2, the Nb_2O_5, and the ZrO_2 nanocoating layers could reduce the recombination rate by constructing the energy barrier at the ZnO/electrolyte interface, leading to the higher V_{OC} values. On the other hand, the TiO_2-nanocoating layers were effective to increase V_{OC} due to the reduction of the surface recombination sites by the grain growth of ZnO as well as the surface passivation. The additional effect of the coating layers was found to be the hindrance of the ZnO grain growth. Consequently the coated ZnO films maintained the high surface area to adsorb a large amount of dyes. For the SiO_2 and the Nb_2O_5 coating, the energy conversion efficiency of the DSSCs increased up to 4.80% and 5.19%, respectively. On the other hand, for the TiO_2 and the ZrO_2 coating, the slight decrease in J_{SC} due to the grain growth led to the lower conversion efficiency. The highest V_{OC} of 0.765 V was recorded for the ZrO_2-coated ZnO electrode due to in the present study. Further work is ongoing to enhance the overall cell performance by optimizing the coating conditions.

Acknowledgment

S. Ueno is grateful for a JSPS Research Fellowship for Young Scientists.

References

[1] M. Grätzel, "Solar energy conversion by dye-sensitized photovoltaic cells," *Inorganic Chemistry*, vol. 44, no. 20, pp. 6841–6851, 2005.

[2] S. Ueno, N. Hitachi, and S. Fujihara, "Nanostructural control of ZnO photoelectrodes for enhancing solar energy conversion efficiency in dye-sensitised solar cells," *International Journal of Nanoparticles*, vol. 4, no. 2-3, pp. 231–247, 2011.

[3] S. Ueno and S. Fujihara, "Effect of an Nb_2O_5 nanolayer coating on ZnO electrodes in dye-sensitized solar cells," *Electrochimica Acta*, vol. 56, no. 7, pp. 2906–2913, 2011.

[4] S. Ueno and S. Fujihara, "Formation of silica nanolayers on ZnO electrodes in dye-sensitized solar cells," *European Journal of Inorganic Chemistry*, no. 14, pp. 2165–2171, 2010.

[5] K. Sayama, H. Sugihara, and H. Arakawa, "Photoelectrochemical properties of a porous Nb_2O_5 electrode sensitized by a ruthenium dye," *Chemistry of Materials*, vol. 10, no. 12, pp. 3825–3832, 1998.

[6] M. Law, L. E. Greene, J. C. Johnson, R. Saykally, and P. Yang, "Nanowire dye-sensitized solar cells," *Nature Materials*, vol. 4, no. 6, pp. 455–459, 2005.

[7] K. Keis, C. Bauer, G. Boschloo et al., "Nanostructured ZnO electrodes for dye-sensitized solar cell applications," *Journal of Photochemistry and Photobiology A*, vol. 148, no. 1–3, pp. 57–64, 2002.

[8] Q. Zhang, T. P. Chou, B. Russo, S. A. Jenekhe, and G. Cao, "Aggregation of ZnO nanocrystallites for high conversion efficiency in dye-sensitized solar cells," *Angewandte Chemie—International Edition*, vol. 47, no. 13, pp. 2402–2406, 2008.

[9] Y. H. Lai, C. Y. Lin, H. W. Chen et al., "Fabrication of a ZnO film with a mosaic structure for a high efficient dye-sensitized solar cell," *Journal of Materials Chemistry*, vol. 20, no. 42, pp. 9379–9385, 2010.

[10] S. Yodyingyong, Q. Zhang, K. Park et al., "ZnO nanoparticles and nanowire array hybrid photoanodes for dye-sensitized solar cells," *Applied Physics Letters*, vol. 96, no. 7, Article ID 073115, 3 pages, 2010.

[11] S. H. Ko, D. Lee, H. W. Kang et al., "Nanoforest of hydrothermally grown hierarchical ZnO nanowires for a high efficiency dye-sensitized solar cell," *Nano Letters*, vol. 11, no. 2, pp. 666–671, 2011.

[12] E. Hosono, S. Fujihara, and T. Kimura, "Synthesis, structure and photoelectrochemical performance of micro/nano-textured ZnO/eosin Y electrodes," *Electrochimica Acta*, vol. 49, no. 14, pp. 2287–2293, 2004.

[13] E. Hosono, S. Fujihara, I. Honma, and H. Zhou, "The fabrication of an upright-standing zinc oxide nanosheet for use in dye-sensitized solar cells," *Advanced Materials*, vol. 17, no. 17, pp. 2091–2094, 2005.

[14] K. Kakiuchi, E. Hosono, and S. Fujihara, "Enhanced photoelectrochemical performance of ZnO electrodes sensitized with N-719," *Journal of Photochemistry and Photobiology A*, vol. 179, no. 1-2, pp. 81–86, 2006.

[15] K. Kakiuchi, M. Saito, and S. Fujihara, "Fabrication of ZnO films consisting of densely accumulated mesoporous nanosheets and their dye-sensitized solar cell performance," *Thin Solid Films*, vol. 516, no. 8, pp. 2026–2030, 2008.

[16] M. Saito and S. Fujihara, "Large photocurrent generation in dye-sensitized ZnO solar cells," *Energy and Environmental Science*, vol. 1, no. 2, pp. 280–283, 2008.

[17] M. Saito and S. Fujihara, "Fabrication and photovoltaic properties of dye-sensitized ZnO thick films by a facile doctor-blade printing method using nanocrystalline pastes," *Nippon Seramikkusu Kyokai Gakujutsu Ronbunshi/Journal of the Ceramic Society of Japan*, vol. 117, no. 1367, pp. 823–827, 2009.

[18] S. Ueno and S. Fujihara, "Controlled synthesis of nanostructured ZnO films for use in dye-sensitized solar cells," *Journal of the Electrochemical Society*, vol. 158, no. 1, pp. K1–K5, 2011.

[19] S. Singh, P. Thiyagarajan, K. Mohan Kant et al., "Structure, microstructure and physical properties of ZnO based materials in various forms: bulk, thin film and nano," *Journal of Physics D*, vol. 40, no. 20, pp. 6312–6327, 2007.

[20] M. Grätzel, "Photoelectrochemical cells," *Nature*, vol. 414, no. 6861, pp. 338–344, 2001.

[21] M. A. Butler and D. S. Ginley, "Prediction of flatband potentials at semiconductor-electrolyte interfaces from atomic electronegativities," *Journal of the Electrochemical Society*, vol. 125, no. 2, pp. 228–232, 1978.

[22] H. P. Maruska and A. K. Ghosh, "A study of oxide-based heterostructure photoelectrodes," *Solar Energy Materials*, vol. 1, no. 5-6, pp. 411–429, 1979.

[23] G. Redmond, A. O'Keeffe, C. Burgess, C. MacHale, and D. Fitzmaurice, "Spectroscopic determination of the flatband potential of transparent nanocrystalline ZnO films," *Journal of Physical Chemistry*, vol. 97, no. 42, pp. 11081–11086, 1993.

[24] T. P. Chou, Q. Zhang, and G. Cao, "Effects of dye loading conditions on the energy conversion efficiency of ZnO and TiO_2 dye-sensitized solar cells," *Journal of Physical Chemistry C*, vol. 111, no. 50, pp. 18804–18811, 2007.

[25] M. K. Nazeeruddin, A. Kay, I. Rodicio et al., "Conversion of light to electricity by cis-X2bis(2,2′-bipyridyl-4,4′-dicarboxylate)ruthenium(II) charge-transfer sensitizers (X = Cl^-, Br^-, I^-, CN^-, and SCN^-) on nanocrystalline TiO_2 electrodes," *Journal of the American Chemical Society*, vol. 115, no. 14, pp. 6382–6390, 1993.

[26] C. H. Ku and J. J. Wu, "Chemical bath deposition of ZnO nanowire-nanoparticle composite electrodes for use in dye-sensitized solar cells," *Nanotechnology*, vol. 18, no. 50, Article ID 505706, 9 pages, 2007.

[27] S. G. Chen, S. Chappel, Y. Diamant, and A. Zaban, "Preparation of Nb_2O_5 coated TiO_2 nanoporous electrodes and their application in dye-sensitized solar cells," *Chemistry of Materials*, vol. 13, no. 12, pp. 4629–4634, 2001.

[28] K. Tennakone, J. Bandara, P. K. M. Bandaranayake, G. R. A. Kumara, and A. Konno, "Enhanced efficiency of a dye-sensitized solar cell made from MgO-coated nanocrystalline SnO_2," *Japanese Journal of Applied Physics, Part 2*, vol. 40, no. 7, pp. L732–L734, 2001.

[29] A. Kay and M. Grätzel, "Dye-sensitized core-shell nanocrystals: improved efficiency of mesoporous tin oxide electrodes coated with a thin layer of an insulating oxide," *Chemistry of Materials*, vol. 14, no. 7, pp. 2930–2935, 2002.

[30] P. K. M. Bandaranayake, P. V. V. Jayaweera, and K. Tennakone, "Dye-sensitization of magnesium-oxide-coated cadmium sulfide," *Solar Energy Materials and Solar Cells*, vol. 76, no. 1, pp. 57–64, 2003.

[31] K. Tennakone, G. R. R. A. Kumara, I. R. M. Kottegoda, and V. P. S. Perera, "An efficient dye-sensitized photoelectrochemical solar cell made from oxides of tin and zinc," *Chemical Communications*, no. 1, pp. 15–16, 1999.

[32] B. L. Cushing, V. L. Kolesnichenko, and C. J. O'Connor, "Recent advances in the liquid-phase syntheses of inorganic nanoparticles," *Chemical Reviews*, vol. 104, no. 9, pp. 3893–3946, 2004.

[33] P. Yang, M. Ando, and N. Murase, "Encapsulation of emitting CdTe QDs within silica beads to retain initial photoluminescence efficiency," *Journal of Colloid and Interface Science*, vol. 316, no. 2, pp. 420–427, 2007.

[34] M. A. Aegerter, "Sol-gel niobium pentoxide: a promising material for electrochromic coatings, batteries, nanocrystalline solar cells and catalysis," *Solar Energy Materials and Solar Cells*, vol. 68, no. 3-4, pp. 401–422, 2001.

[35] S. D. Meetei, S. D. Singh, and V. Sudarsan, "Polyol synthesis and characterizations of cubic ZrO_2:Eu^{3+} nanocrystals," *Journal of Alloys and Compounds*, vol. 514, pp. 174–178, 2012.

[36] Y. Du, M. S. Zhang, J. Hong, Y. Shen, Q. Chen, and Z. Yin, "Structural and optical properties of nanophase zinc oxide," *Applied Physics A*, vol. 76, no. 2, pp. 171–176, 2003.

[37] S. Ueno and S. Fujihara, "Influence of sintering behavior of ZnO nanoparticles on J-V characteristics of ZnO-based dye-sensitized solar cells," *Key Engineering Materials*, vol. 445, pp. 117–120, 2010.

[38] E. Palomares, J. N. Clifford, S. A. Haque, T. Lutz, and J. R. Durrant, "Control of charge recombination dynamics in dye sensitized solar cells by the use of conformally deposited metal oxide blocking layers," *Journal of the American Chemical Society*, vol. 125, no. 2, pp. 475–482, 2003.

[39] F. Lenzmann, J. Krueger, S. Burnside et al., "Surface photovoltage spectroscopy of dye-sensitized solar cells with TiO_2, Nb_2O_5, and $SrTiO_3$ nanocrystalline photoanodes: indication for electron injection from higher excited dye states," *Journal of Physical Chemistry B*, vol. 105, no. 27, pp. 6347–6352, 2001.

[40] K. Tennakone and J. Bandara, "Multiphoton semiconductor photocatalysis," *Solar Energy Materials and Solar Cells*, vol. 60, no. 4, pp. 361–365, 2000.

[41] R. Katoh, A. Furube, T. Yoshihara et al., "Efficiencies of Electron Injection from Excited N3 Dye into Nanocrystalline Semiconductor (ZrO_2, TiO_2, ZnO, Nb_2O_5, SnO_2, In_2O_3) Films," *Journal of Physical Chemistry B*, vol. 108, no. 15, pp. 4818–4822, 2004.

[42] M. Law, L. E. Greene, A. Radenovic, T. Kuykendall, J. Liphardt, and P. Yang, "ZnO-Al_2O_3 and ZnO-TiO_2 core-shell nanowire dye-sensitized solar cells," *Journal of Physical Chemistry B*, vol. 110, no. 45, pp. 22652–22663, 2006.

[43] Y. Y. Xi, Y. F. Hsu, A. B. Djurišić, and W. K. Chan, "Electrochemical synthesis of ZnO nanoporous films at low temperature and their application in dye-sensitized solar cells," *Journal of the Electrochemical Society*, vol. 155, no. 9, pp. D595–D598, 2008.

[44] F. Fabregat-Santiago, J. García-Cañadas, E. Palomares et al., "The origin of slow electron recombination processes in dye-sensitized solar cells with alumina barrier coatings," *Journal of Applied Physics*, vol. 96, no. 11, pp. 6903–6907, 2004.

[45] H. Chen, A. Du Pasquier, G. Saraf, J. Zhong, and Y. Lu, "Dye-sensitized solar cells using ZnO nanotips and Ga-doped ZnO films," *Semiconductor Science and Technology*, vol. 23, no. 4, Article ID 045004, 6 pages, 2008.